The interaction of mercury and methylmercury with chalcogenide nanoparticles

Xudong Wang[a], Emily Seelen[bd], Nashaat Mazrui[abe], Peter Kerns[a], Steven L. Suib[ac], Jing Zhao[ac] and Robert Mason*[b]

[a] Department of Chemistry, University of Connecticut, 55 North Eagleville Rd., Storrs, USA

[b] Department of Marine Sciences, University of Connecticut, Groton, CT, USA

[c] Institute of Materials Science, University of Connecticut, 97 North Eagleville Rd., Storrs, USA

[d] Current address: Department of Earth Sciences, University of Southern California, CA, USA

[e] Current address: Okavango Research Institute, Botswana

* Corresponding author: Email: robert.mason@uconn.edu

Abstract

Mercury (Hg) and methylmercury (CH_3Hg) bind strongly to micro and nano (NP) particles and this partitioning impacts their fate and bioaccumulation into food webs, and, as a result, potential human exposure. This partitioning has been shown to influence the bioavailability of inorganic Hg to methylating bacteria, with NP-bound Hg being more bioavailable than particulate HgS, or organic particulate-bound Hg. In this study we set out to investigate whether the potential interactions between dissolved ionic Hg (Hg^{II}) and CH_3Hg and NPs was due to incorporation of Hg into the core of the cadmium selenide and sulfide (CdSe; CdS) nanoparticles (metal exchange or surface precipitation), or due purely to surface interactions. The interaction was assessed based on the quenching of the fluorescence intensity and lifetime observed during Hg^{II} or CH_3Hg titration experiments of these NP solutions. Additional analysis using inductively coupled plasma mass spectrometry of CdSe NPs and the separated solution, obtained after Hg^{II} additions, showed that there was no metal exchange, and X-ray photoelectron spectroscopy confirmed this and further indicated that the Hg was bound to cysteine, the NP capping agent. Our study suggests that Hg and CH_3Hg adsorbed to the surfaces of NPs would have different bioavailability for release into water

or to (de)methylating organisms or for bioaccumulation, and provides insights into the behavior of Hg in the environment in the presence of natural or manufactured NPs.

Capsule

The study examined the interactions of inorganic mercury and methylmercury with capped CdSe and CdS nanoparticles to examine how these interactions affect their environmental reactivity and bioavailability

Keywords: mercury, methylmercury, nanoparticles, cadmium selenide, cadmium sulfide

1. Introduction

Mercury (Hg) pollution is a global environmental problem with elevated levels of Hg being found in many aquatic systems due to the enhanced inputs of Hg from local and global anthropogenic sources (Driscoll et al., 2013; Outridge et al., 2018). Increased Hg inputs into the environment are a human health issue due to its conversion into methylmercury (CH_3Hg) in aquatic systems. CH_3Hg is considered the most toxic form of Hg as it is bioaccumulated more readily than inorganic Hg and biomagnified in local aquatic food webs, impacting human health through fish and seafood consumption (Sunderland et al., 2018; Mahaffey et al., 2011). As CH_3Hg exposure results in negative effects to the human brain, growing fetal cells, kidney and neurological systems, the developing fetus and young children are the most susceptible to health impacts imparted from CH_3Hg exposure. Additionally, communities with high seafood consumption and/or living in contaminated areas may also be susceptible to health effects from long-term or high dose CH_3Hg exposure (Zahir et al., 2005).

In aquatic environments, inorganic Hg can be converted to CH_3Hg and even dimethylmercury ($(CH_3)_2Hg$), mostly via microbial pathways (Benoit et al., 2003; Gilmour et al., 2013; Podar et al., 2015; Regnell and Watras, 2019). Most methylating bacteria are anaerobic (e.g. sulfate-reducing

and iron-reducing bacteria) and methylation rates have been shown to be the greatest at redox transition zones, hence sediments and flocculated organic matter are often focused on as sites for methylation (Gilmour et al., 2013; Regnell and Watras, 2019; Schartup et al., 2013; 2014). The rate of mercury methylation is a function of the speciation and bioavailability of the inorganic Hg to the methylating organisms responsible for this conversion (Benoit et al., 2003). For example, binding of inorganic Hg (Hg^{II}) to dissolved/particulate natural organic matter (NOM) can make Hg more or less bioavailable for methylation depending on the source and concentration of NOM, and the type of interaction, as well as other redox conditions of the methylating environment as Hg binds strongly with sulfide (Graham et al., 2013; Jonsson et al., 2012; Hsu-Kim et al., 2013; Mazrui et al., 2016). While Hg can be precipitated as micro and nano HgS particles in highly sulfidic environments, Hg and CH_3Hg can also bind strongly to inorganic micro and nano particles (NPs), such as metal sulfides and selenides, due to their abundant binding sites resulting from their high relative surface area (Mazrui et al., 2016; Zhang et al., 2014; Hsu-Kim et al., 2013; Rivera et al., 2019). The binding of inorganic Hg to micro and NPs have been shown to directly influence the degree of Hg methylation (Jonsson et al., 2012; Mazrui et al., 2016; Zhang et al., 2012; 2014; Graham et al., 2012; Ndu et al., 2018). Overall, micro HgS is less bioavailable to methylating organisms than Hg^{II} that is either inorganically complexed, present as HgS NPs, or bound to dissolved (DOC) or particulate (POC) natural organic carbon in the water column. The reason for the higher bioavailability of HgS NPs is a focus of current research (Rivera et al., 2019; Zhang et al., 2019).

Most studies (Gerbig et al., 2011; Hsu-Kim et al., 2013; Pham et al., 2014; Poulin et al., 2017; Slowey et al., 2010; Zhang et al., 2012; 2014; 2019) have focused on HgS NPs and their bioavailability, but there is the potential for dissolved Hg^{II} and CH_3Hg ions and complexes to interact with other micro or NPs in the environment, both natural and manufactured, particularly those composed of heavy metals (e.g. Zn, Cd, Pb) and Group 16 metalloids (S, Se and Te) (Van Leeuwen et al., 2017). Rivera et al. (2019) showed that the type of interaction between Hg and FeS particles – adsorption or co-precipitation – influenced the solubilization of the Hg from the particles. Additionally, however, they found that the degree of solubilization was not a good predictor of methylation likely because of the unique environment that develops when methylating bacteria are closely associated with the particulate surface. These studies were done in the absence of organic matter which obviously influences the surface interaction. It has not been adequately

demonstrated for nanoparticles capped with an organic ligand whether the adsorbed Hg would remain as a surface complex, or whether the Hg could replace the core metal, and what is the influence of the capping agent on this interaction. An exchange reaction leading to Hg co-precipitation would be thermodynamically favorable given the resultant formation of Hg-S or Hg-Se bonds, depending on the nature of the NP (log K_{sp} values for the reaction: $MX(s) = M^{2+} + HX^{-}$ are: for HgS -39.5; CdS -14.3; HgSe -45.5; CdSe -19.8). Jeong et al. (2007; 2010) showed that adsorption of Hg^{II} to uncoated FeS NPs occurred at low Hg/Fe ratios (<0.05) and that precipitation of Hg as HgS occurred only at higher ratios. Rivera et al. (2019) found that the rate of methylation depended on the degree of Hg-S coordination in the particle matrix. For CH_3Hg, the interaction with micro sulfide phases resulted in chemical transformation (Jonsson et al., 2016) with the CH_3Hg being converted to $(CH_3)_2Hg$ in the presence of either FeS, CdS and HgS, and a similar reaction pathway has been proposed by others, where a complex of the form $(CH_3Hg)_2S$ degrades releasing $(CH_3)_2Hg$ (Craig and Bartlett, 1978). The results of Jonsson et al. indicated that the interaction was a surface reaction. Additionally, the formation of $(CH_3)_2Hg$ has also been shown to occur in the presence of thiols and Se-containing organic compounds (Jonsson et al., 2016; Asauzzaman and Schreckenbach, 2011; Khan and Wang, 2010). It is not known whether such methyl transfer reactions would occur in the presence of NPs of the same core composition.

When HgS co-precipitation occurs in the experiments discussed above, a metal exchange reaction occurs and this has been shown to also happen during the manufacture of quantum dots containing more than one metal (Gupta et al., 2013; Choi et al., 2017). In these exchange reactions, the concentrations of both metals are high, and the Cd/Hg ratio ranges from 0.1 to 1, or greater in these mixed CdHgSe and CdHgTe quantum dots. These ratios are consistent with, but at higher ratios than, the results discussed above, likely because of the presence of capping agents in the manufacture of these NPs. The potential for this to occur under environmental conditions has not been adequately studied.

Also, as discussed above, the form of interaction – surface adsorption/complexation versus co-precipitation – would, because of differences in the binding strength of these associations, dramatically influence the bioavailability of any Hg or CH_3Hg associated with chalcophile surfaces to the water column and methylating organisms (Manceau et al., 2015; Hofacker et al., 2013; Rivera et al., 2019). Surface complexation of Hg could explain why HgS NPs stimulate

more Hg methylation than the micro HgS particles (Mazrui et al., 2016), although most of the studies examining Hg methylation in the presence of nanoparticles suggest a complex interaction between the methylating bacteria and the surface of the NPs (Zhang et al., 2019; Rivera et al., 2019).

Additionally, in natural environments, uncoated particles are unlikely as they would rapidly become coated with NOM, so more studies examining the interactions of Hg^{II} and CH_3Hg with organically-coated particles are needed. Studies have suggested that the unsaturated surface atoms and various functional groups associated with the capping ligands of NPs can influence their reactivity and complexation with metals in solution (Zhang et al., 2012; Van Leeuwen et al., 2017; Pham et al., 2014). With the increasing production and application of nanomaterials, and their presence in the environment naturally, the study of interactions between Hg^{II} and CH_3Hg with coated NPs allow us understand the role of NPs in CH_3Hg transformation and Hg^{II} methylation in the environment, and to understand how to better control the impact of Hg pollution in the future.

Our study therefore focused on how Hg^{II} and CH_3Hg species interact with NPs, to inform our understanding of their bioavailability in aquatic systems. We used aqueous CdSe and CdS NPs capped with L-cysteine as model systems, as this allowed an evaluation of whether there is a metal exchange reaction occurring between the Hg species in solution and the NP core metal, at the relative concentrations used here (Hg:Cd <0.05). Given that the core metal did not influence the interactions of CH_3Hg with micro metal sulfide particles (Jonsson et al., 2016), we inferred that the same would be true for NPs and that our studies would be applicable to other metal-sulfide/selenide NPs as well, although the thermodynamics of the interaction would favor a metal exchange reaction for Hg if Cd is the core metal. We hypothesized that the interaction of Hg^{II} and CH_3Hg in our experiments would be influenced by both the particle size and type of interaction occurring within or on the surface of the NP. The interaction could differ depending on the type and formulation of the NP. To address this specifically, we examined whether the interaction of Hg and CH_3Hg with the NPs was due to incorporation into the NP core (metal exchange or co-precipitation), or purely due to surface interactions. Briefly, inorganic Hg and CH_3Hg were added to CdS and CdSe NP solutions, and the interaction was assessed based on a decrease in fluorescence intensity and its lifetime observed during the Hg/CH_3Hg titration experiments due to fluorescence quenching. Additionally, inductively coupled plasma mass spectrometry (ICP-MS)

and X-ray photoelectron spectroscopy (XPS) were used to further examine how the metal ions partitioned after the reaction was completed. Our results suggested that no HgS precipitation or metal exchange reaction occurred, except at very high Hg to Cd ratios where HgS or HgSe precipitated, consistent with the results of others (Gupta et al., 2013; Jeong et al., 2010; Zhang et al., 2019) and that the Hg/CH_3Hg was bound to the amine and carboxylate groups of the L-cysteine capping agent on the NP surface.

The overall results were that dissolved Hg^{II} and CH_3Hg interacted with the organic matter surface moieties of the NP rather than with the NP core. Therefore, the bioavailability of Hg^{II} associated with NPs, when the ratio of Hg to the core metal is low, is likely more strongly dictated by the NP surface binding ligands than the composition of the metal core itself. Furthermore, such interactions would suggest that the reactions leading to the formation of $(CH_3)_2Hg$ on the surface of micro sulfide particles examined by Jonsson et al. (2016) are not likely to occur with organic matter coated micro particles or NPs. These results inform our understanding of the biogeochemical cycling of Hg and CH_3Hg in the natural environment given that uncoated metal sulfide/selenide particles are unlikely, and that coated NPs would behave differently during interactions with dissolved cations.

2. Experimental

2.1 Materials

Cadmium chloride (Technical grade), sodium sulfite (≥98%), selenium powder (99.99%), sodium hydroxide (≥97.0%), L-cysteine hydrochloride monohydrate (≥99.0%) and mercury (II) chloride (≥98%) were all purchased from Sigma-Aldrich. Ethanol (200 proof) was purchased from J. T. Baker. Methylmercury standard (1000 ppm in HCl) was purchased from Alfa Aesar. All chemicals were used as received.

2.2 The Synthesis and Purification of Aqueous CdSe Nanoparticles

To prepare the reaction precursor (Na_2SSeO_3), 37 mg of selenium (Se) powder, 605 mg of sodium sulfite (Na_2SO_3) and 25 mL of water were mixed in a flask. The mixture was kept at 85 ℃ with

stirring and nitrogen (N_2) protection overnight until a colorless transparent solution was obtained. For the CdSe NP formation, under a nitrogen atmosphere, 20.0 mL of deionized water, 0.783 mL of sodium hydroxide (NaOH) solution (1M), 0.058g of L-cysteine hydrochloride monohydrate, 0.25 mL of 0.15 M cadmium chloride ($CdCl_2$) were added into a glass flask within 10 min with stirring. After 10 min, 5.0 mL of Na_2SSeO_3 precursor was added into the reaction mixture which was kept stirring mildly for 1.5-2 h while sparging with N_2. The reaction solution gradually changed from colorless to yellow.

For purification of the NPs, the CdSe solution was mixed with ethanol with the volume ratio (CdSe solution: ethanol) of 3:1 and centrifuged at 7000 rpm for 10 min. The supernatant was discarded and then 9 mL of DI water was added to redisperse the precipitate. The redispersed CdSe nanoparticle solution was then sonicated for at least 1 min to ensure dispersion of NPs prior to the Hg^{II}/CH_3Hg additions.

2.3 Nanoparticle Characterization

The synthesis of the CdS nanoparticles is detailed in the Supporting Information (Mazrui, 2016). Based on our analysis of the CdSe NPs by ICP-MS, detailed below, the average amount of Cd in the NPs was 3.3 μmoles. The release of Cd from the CdSe NPs into solution after their centrifugation and resuspension into water was also characterized by ICP-MS. Overall, less than 1% of the Cd was found in solution and the concentration was independent of the addition of Hg to the NP solutions (Table 1). The size of the CdSe NPs was determined using a transmission electron microscope (Fig. 1B). For characterization, UV-Vis spectra were measured either with a Cary 60 (Agilent Technologies) or Hitachi U3010 UV-Vis spectrometer (Fig. 1A).

The relative ratio of Hg to Cd used in the titration experiments (<0.05) was chosen to simulate the level of interaction likely under environmental conditions where the ratio of dissolved and particulate species is small (partition coefficients for Hg are ~10^5 - 10^6 L/kg; Mason, 2013). Photoluminescence spectra were taken on a Horiba Fluomax Plus fluorometer with the excitation at 400 nm for the CdSe NP titrations with Hg^{II} and with a Cary Eclipse Agilent instrument for those with CH_3Hg. A Hitachi F2000 instrument was used to examine the interactions of CdS NPs and Hg^{II}, with excitation of 350 nm.

198 The time-dependent fluorescence decays were acquired with a home-built set-up. A pulsed laser
199 at 405 nm (PicoQuant, ~100−120 ps pulse duration, 2.5 MHz repetition rate) was used to excite
200 samples with different concentration of mercury ions added. The photoluminescence signal of the
201 solutions was acquired through a 20× air objective (Nikon, N.A. = 0.45) and sent to a single-photon
202 detector (τSPAD, PicoQuant) after signal cutoff by an appropriate spectral filter. The
203 photoluminescence decay data were collected using a time-correlated single-photon counting
204 (TCSPC) module (PicoHarp 300, PicoQuant) with a time resolution of 32 ps. All the optical
205 spectroscopy experiments were performed under ambient conditions.

206 *2.4 ICP-MS*

207 To obtain both the dissolved and particulate phases following the addition of Hg^{2+} to CdSe NP
208 solutions, the NPs in the solutions were separated from the supernatant by adding 1 M $CaCl_2$
209 solution and then centrifuging to enhance the precipitation of the NPs (Mazrui et al., 2018). The
210 separated NPs, dissolved in 10% nitric acid, and the acidified supernatant were analyzed for Hg
211 and Cd using ICP-MS to determine whether the metals were associated with the NPs, and to
212 ascertain if there had been any exchange between Hg and Cd within the NPs. To determine the
213 extent that the added $CaCl_2$ would cause removal of Hg from solution, it was also added to a stock
214 Hg solution as a control. Less than 3% of the Hg was removed from the solution by the
215 precipitation of the $CaCl_2$ (Table 1), in comparison to the removal of essentially all the Hg in the
216 solutions containing CdSe NPs. As both the precipitated NPs and the remaining solution were
217 analyzed in most cases, the added Hg and the total Cd were accounted for. For Cd, there was some
218 variability in the total Cd concentration between solutions from the different experiments (Table
219 1), which reflects the variation in the amount of Cd recovered during the centrifugation and
220 resuspension step prior to the Hg addition, as discussed above. The concentrations of Hg in the
221 solutions were also checked through analysis using a Nippon Direct Mercury Analyzer.

222 *2.5 X-Ray Photoelectron Spectroscopy*

223 Samples of NPs, with or without moderate levels of Hg added, were mixed with ethanol and
224 separated using high speed centrifugation as described above without the addition of any other
225 chemicals to the medium for X-ray photoelectron spectroscopy (XPS) characterization. The
226 samples were dropped onto silicon wafer, dried and then pressed onto double sided carbon tape,

mounted on an Al coupon pinned to a sample stage with a washer and screw then placed in the analysis chamber. The analysis of these CdSe-Hg NPs was done on a PHI model Quantum 2000 spectrometer with a scanning ESCA multiprobe (F Physical Electronics Industries Inc.), using Al Kα radiation (λ=1486.6 eV) as the radiation source. The spectra were recorded in the fixed analyzer transmission mode with pass energies of 187.85 eV and 29.35 eV for recording survey and high resolution spectra, respectively. Binding energies (BE) were measured for C 1s, N 1s, O 1s, Se 3d and Cd 3d. The XPS spectra obtained were analyzed and fitted using CasaXPS software (version 2.3.16). Sample charging effects were eliminated by correcting the observed spectra with the C 1s BE value of 284.8 eV.

3. Results and Discussion

3.1 Nanoparticle Synthesis and Characterization

The synthesis of aqueous CdSe NPs was based from a reported method (Park et al, 2010) in which L-cysteine was used as the capping ligand due to the strong binding between the thiol group and surface Cd atoms of the CdSe NPs. To shorten the reaction time, the molar ratio of Na_2SO_3 to Se (10:1) in the preparation of Na_2SSeO_3 was increased relative to that (3:1) in the reference. The excess Na_2SO_3 served as a mild reducing agent to complete the growth of CdSe NPs within a few hours instead of several days. A basic pH of the reaction solution is desired so that the carboxylic group of L-cysteine are deprotonated, and therefore negatively charged as the electrostatic repulsion is crucial to keep the aqueous CdSe NPs stable and of small diameter. Meanwhile, $Cd(OH)_2$ and other cadmium hydroxide complexes would form with a pH value beyond 12.5, which would interfere with the growth of Cd based nanocrystals (Jing et al., 2016). The optimal pH for the growth of CdSe NPs in our case was around 10.9. As shown in Figure 1, the narrow and intense first extinction peak at 420 nm appeared at the end of the reaction with freshly made Se precursor at pH 10.87. The diameter of CdSe under the optimal condition was estimated to be ~1.7 nm using an empirical size fitting function reported by Yu et al. (2003). In the reactions with higher pH or aged Se precursor, peak broadening and red-shift were observed, indicating a larger size dispersity of the CdSe NPs. The size of the CdSe NPs was also determined using TEM (Fig. 1B) and a size of 1.9 ± 0.3 nm was determined.

The CdS NPs were made using the approach developed by Mazrui et al. (2016) for the manufacture of HgS NPs. Their UV-vis spectrum has a peak at 372 nm (Fig. S1) and the particle size was calculated as 3.5 nm using the effective mass approximation theory. From TEM images (Fig. S2), a diameter of 3.0 ± 0.4 nm was estimated, which matches the calculation based on the UV-vis peak.

3.2 Interaction of mercury with the nanoparticles examined by spectroscopy

Heavy metal ions are good photoluminescence quenchers. There are mainly two models responsible for the quenching of fluorescence (Fraiji et al., 1992). In the dynamic quenching model, the decrease in fluorescence is caused by collision of a free quencher with a fluorophore. In this process, energy transfer or electron transfer occurs from the excited state of the fluorophore to the quencher. With a pure dynamic quenching process, the quenching should follow the Stern-Volmer equation shown in equation 1. Here I_0 and I are the fluorescence intensities with and without addition of the quencher (Hg^{II} of CH_3Hg), respectively; k_q represents the quenching rate constant ($M^{-1}s^{-1}$); τ_0 is the lifetime of the excited state of the fluorophore in the absence of the quencher (s); and [Q] is the quencher concentration. According to this relationship, I_0/I vs. $[Q]$ should follow a linear relationship:

$$\frac{I_0}{I} = 1 + k_q \tau_0 [Q] \quad (1)$$

On the other hand, if the interaction involves a static quenching process, the quencher and the fluorophore form a ground state complex which is hard to break and excite. In this case, a drop of fluorescence intensity will also be observed with the addition of quencher due to fewer excitable ground state fluorophores, but for a different reason. Similar to dynamic quenching, a plot of I_0/I vs. [Q] also has a linear relationship, where the slope is K_a, the association constant of the fluorophore-quencher complex (equation 2) (Fraiji et al., 1992):

$$\frac{I_0}{I} = 1 + K_a [Q] \quad (2)$$

The study of the fluorescence quenching process of CdSe and CdS due to the addition of Hg^{II} or CH_3Hg can therefore provide insight into the interaction between the ions and the NPs. Here, we measured both steady state spectra and fluorescence decays of fixed amounts of CdSe NP solutions

with gradual addition of Hg^{II} or CH_3Hg. Similar studies were previously done with CdS NPs (Fig. S3A & S3B) (Mazrui, 2016) although the extent of the Hg addition was smaller. As shown in Fig. 2A (top black curve) and Fig. S3A, the photoluminescence spectra of CdSe and CdS NPs was very broad, with a peak maximum at 560 nm and 540 nm, respectively.

The broad and long-wavelength features of the PL spectrum indicate that the emission came from surface trap states instead of band-gap radiative recombination of excitons (Yu et al., 2012). When $HgCl_2$ spikes were added to purified L-cysteine capped CdSe and CdS NP solutions, the fluorescence peak intensity dropped without shifting the peak position (Figs. 2A and S3A). The Stern-Volmer plot for the Hg-CdSe studies showed a nonlinear curve in Fig. 2B, indicating a mixed quenching mechanism. For the lower level Hg^{II} additions to the CdS NP solution, the curve is linear (Fig. S3B), similar to the initial curve for the CdSe study (Fig. 2B).

The relationships found suggest that Hg^{II} can quench both the excited state and ground state of CdSe NPs in our experiment. The observation is different from the quenching process reported in the literature (Ding et al., 2015; Duan et al., 2009; Paim et al., 2017). Previous studies have mostly reported static quenching of the fluorescence of aqueous quantum dots by metal ions. The relationship between I_0/I and [Q] appears relatively linear at low Hg^{II} concentrations, and suggests that there may be dominantly static quenching in these cases. In contrast, the mechanism is different at higher concentrations with more dynamic quenching occurring. For the low Hg^{II} additions with the CdSe NPs (Fig. 2B), a slope of 0.147 μM^{-1} ($r^2 = 0.995$) was determined ($K_a = 1.47 \times 10^5\ M^{-1}$). However, this value may be inaccurate due to there being two processes occurring. If both quenching processes are occurring, then the overall relationship is given by (Fraiji et al., 1992):

$$\frac{I_0}{I} = (1 + k_q\tau_0[Q])(\ 1+ K_a[Q]) = 1+ (K_D + K_a\ )[Q] + K_DK_a\ [Q]^2 \qquad (3)$$

where $K_D = k_q\tau_0$. By diving eq. 3 through by [Q], a linear relationship is found:

$$(\frac{I_0}{I} - 1)/[Q] = \ K_DK_a[Q] + (K_D + K_a) \qquad (4)$$

with a slope of K_DK_a and an intercept of (K_D + K_a). From a plot of all the data, which exhibited higher variability given the associated errors in all the calculated values, the following values

were determined: $K_a = 1.52 \times 10^6\ M^{-1}$ and $K_D = 0.0163\ \mu M^{-1}$. The initial lifetime without Hg addition, τ_0, is 6.3 ns, estimated by a stretched exponential fitting since the decay was not a simple mono-exponential decay. Thus $k_q = K_D/\tau_0 = 2.60 \times 10^{12}\ M^{-1}s^{-1}$. The estimated value for K_a with this linearization of the data is an order of magnitude higher than the previous estimate based on the initial curve assuming a sole static quenching mechanism, and likely more closely represents the true value.

Similarly, the study with CdS NPs and Hg^{II} (Fig. S3A) also showed a linear relationship for the low concentrations tested (Fig. S3B) and the initial slope of the relationship is similar to that for the low concentration additions for the CdSe NPs: slope = $2.7 \times 10^5\ M^{-1}$. The similarity in the values estimated in this manner suggests that these constants reflect an interaction that is not primarily due to the NP core but to the surface properties, which is consistent with the notion of a static quenching effect, and an interaction of Hg^{II} with the capping agent, which is the same for both NPs. For the CdS NP experiments there were insufficient measurements to deconvolute the signal further. Overall, at low concentration, static quenching is the main mechanism occurring but that at higher concentrations both forms of quenching mechanisms are important.

To confirm whether dynamic quenching was involved, time-dependent fluorescence decay experiments were performed on the CdSe NPs with Hg^{II} addition (Fig. 3A & 3B). In the static quenching process, the formation of a fluorophore-quencher complex will not affect the recombination dynamics of excitons, thus the fluorescence lifetime will be independent of the quencher. However, in the dynamic quenching model, the presence of the quencher will provide additional non-radiative recombination channels of the excited fluorophore, resulting in a shorter lifetime. Figure 3A clearly showed that the fluorescence decay rate was higher with the increasing concentrations of the added Hg^{II}, and that there was less of an effect at low concentrations compared to higher concentrations. These results suggest that static quenching is dominating at the lower Hg addition concentrations due to a much larger K_a value compared to K_D, but also that there is dynamic quenching occurring for all added Hg concentrations.

In Figure 3B, the Stern-Volmer fitting with τ_0/τ vs. the concentration of quencher gave a non-linear curve. The non-zero slope of the Stern-Volmer plot confirmed that there was a dynamic quenching process involved in the quenching of CdSe NPs by Hg^{II}. Similar studies of the fluorescence decay

with the CdS NPs showed a similar small effect on the lifetime of the decay given the low concentrations of the Hg^{II} additions (Fig. S3C; Mazrui, 2016). These results further confirm that the interactions are similar for Hg in the presence of either the CdSe or the CdS NPs, suggesting the mechanism is not related to the core of the NP but is an interaction with the surface capping agent. Further experiments were also conducted using the CdSe NPs with the addition of CH_3Hg (Fig. 4A & 4B). Quenching was again observed, with a pattern similar to that obtained with addition of Hg^{II} (Fig. 2A & 2B). Again, at low concentrations of added CH_3Hg, the relationship was linear with a slope of 0.152 μM^{-1} ($r^2 = 0.991$), lower than found for the Hg^{II} additions. Using equation 4, the following results were obtained for the constants: $K_a = 7 \times 10^4\ M^{-1}$ and $K_D = 5.6 \times 10^4\ M^{-1}$, or $k_q = 8.9 \times 10^{12}\ M^{-1}s^{-1}$. The value of K_a is lower for CH_3Hg, which could be expected as this species generally binds less strongly than inorganic Hg (Table S1).

The K_a values estimated here are conditional constants and the actual formation constants would depend on the speciation of Hg^{II} and CH_3Hg in the medium, and the ligands/sites to which the cations are binding to in the NP. Overall, the differences in the value of the conditional stability constants are consistent with their known binding strength, i.e. Hg^{II} typically forms somewhat stronger complexes with ligands than CH_3Hg (Table S1). Additionally, the similarity in the values of K_a for the interaction of Hg^{II} with the different NPs is consistent with the fact that the interaction is occurring with the capping agent, which is similar in all experiments. To convert the conditional stability constants into formation constants would require knowledge not only of the solution speciation, but also the concentration of the surface ligands on the NPs, and the surface charge on the NPs, if the interaction is indeed with the capping agent only. These were not measured in the current study. However, the estimated K_a values are much lower relative to that of Hg^{II} and CH_3Hg binding to sulfide or thiols ($\log\beta_1 > 10$), that even though the dissolved speciation of Hg and CH_3Hg is not taken into account, one could conclude that the binding in our experiments is not to reduced sulfur or selenide ligands.

Overall, the mixed quenching mechanism, as demonstrated above, suggests that a specific interaction between Hg^{II} and CH_3Hg and the L-cysteine capped CdSe and CdS NPs was responsible for the formation of ground state CdSe-Hg, CdSe-$HgCH_3$ or CdS-Hg complexes. There could be two kinds of interactions in the NP-Hg system. Firstly, the Hg ion could bind to functional groups of the L-cysteine, such as the amine group and the carboxylic acid group, which

is suggested by the results above. The thiol group is likely involved in the interaction with the NP core – binding to the Cd^{II}. Secondly, the Hg could possibly exchange with the Cd atoms in the core part of CdSe NPs resulting in the formation of CdSe-HgSe NPs, or the sulfide analogs. If the interaction was the latter case, when Hg^{II} was added to CdSe NP solution, the exchange reaction would result in an increase in Cd^{II} in the supernatant after precipitation and separation of the NPs. This was investigated using ICP-MS.

3.3 Examination of mercury and cadmium distribution between the solution and the nanoparticles

To study further how the Hg ions were interacting with the CdSe NPs, we separated the NPs, and analyzed each component by ICP-MS to quantify Hg and Cd in both the supernatant and associated with the precipitated CdSe NPs from the solutions with different concentrations of $HgCl_2$ added. The data are presented in Table 1. The results strongly suggest that essentially all the Hg was associated with the NPs (i.e. found in the precipitate) and that the amount of Hg ions added did not impact the Cd concentration in the NPs or in solution. The measured amount of total Cd in each vial agrees well with our calculation of the Cd present, based on the NP synthesis. There was always much more Cd than Hg in the precipitate (Hg:Cd <0.05). The $CaCl_2$ was also added to the 10 μM Hg stock solution and after centrifugation, 97.7% of the Hg was still in solution indicating that the removal of Hg due to the addition of the $CaCl_2$ was minimal, as expected, and so the removal in the other solutions was due to the association of Hg with the NPs.

In one case, when a very high concentration of 290 μM Hg was added, a black precipitate, which was likely HgSe, formed (all the Hg but no Cd was found in the precipitate when analyzed using ICP-MS), indicating that at sufficient Hg concentration, the Hg does replace the Cd but in forming micro particles and not nanoparticles. In a separate experiment, a black precipitate of supposedly HgS also formed when an equivalent amount of Hg^{2+} to Cd (1.5 mM) was added to a CdS NP solution.

There are a number of conclusions that can be drawn from the fluorescence and ICP-MS data. Firstly, Hg^{II} and CH_3Hg are binding to the NPs and changing their fluorescence, but they are not exchanging with Cd^{II} in the matrix (core) of the NP. Rather, there is either a surface reaction with the Se/S sites on the surface of the NP, or the Hg is only interacting with the ligand (L-cysteine). The fluorescence spectra plots suggest the latter is occurring due to no shift of the PL maximum

wavelength during the quenching experiments. Finally, in the case where the black precipitate was observed, there was no Cd in the precipitate (data not shown in Table 1). Therefore, at a high enough Hg concentration, a cation exchange did occur and essentially the CdSe NPs were converted into HgSe micro particles and precipitated from solution.

3.4 Characterization of nanoparticle surface interactions

To further explore the potential interactions, XPS was used to identify the interaction between Hg and the surface of CdSe NPs at moderate Hg concentrations after separation of the NPs by high speed centrifugation (Fig. 5). Potential binding sites of L-cysteine are thiol, amine and carboxylic groups. Thiol groups would typically be bound to the surface Cd atoms of the CdSe NPs. If Hg competed with Cd for binding to the thiol, there would be a high percentage of Hg-L-cysteine complex present in the supernatant. Our data indicated that mostly over 99% of the Hg was associated with the CdSe NPs, which excluded this binding mechanism. Thus, we examined by XPS whether Hg was binding to the O in the carboxylate group or to the N in the amine group, and whether there were any interactions with the Se or Cd. The black line in the XPS spectra of CdSe NPs (Figure 5A) showed that the O 1s spectrum had two peaks at 533.67 eV and 531.51 eV, representing the different oxidation states of oxygen atoms in the carboxylate group. After the addition of ~33 μM of $HgCl_2$, the binding energy peaks shifted to a single peak at 532.71eV, showing that there were two symmetric oxygen atoms in the carboxylate moiety. This peak change suggested that Hg is bound to two equivalent oxygen atoms of the carboxylate group via a bidentate bond (Wu et al., 2004). In addition, the N 1s spectrum peak in Figure 4B shifted towards higher binding energy after the addition of $HgCl_2$, even though the N 1s signal was masked partially by the nearby Cd 3d 5/2 peak. The shift of the N 1s peak resulted from the increase of the oxidation state of the N atom caused by the addition of Hg. Shifting to a higher binding energy is indicative of electron donation of N to Hg, indicating the binding between the Hg and the N atom of the amine group.

To investigate whether the Hg was bound to the surface Se atoms, the XPS data of Se 3d and Cd 3d were also collected. There was only a negligible shift of the Se 3d peak caused by Hg (Figure S4A in SI), which indicated there was no binding between the surface Se and Hg. Moreover, the XPS spectra of Cd 3d showed no shift (complete overlap) with and without Hg ion addition (Figure

S4B in SI). If there was Hg bound to Se atoms on the surface of CdSe NPs, a shift in the binding energy peaks of Cd 3d should have been observed because of the competitive binding of Hg. The XPS data of the Se 3d and Cd 3d spectra consistently showed that there was no interaction between Hg and Se atoms. Thus, Hg was bound to the oxygen atoms of the carboxylate group and the N atom of the amine group. This finding is consistent with the observed mixed quenching process. The formation of the CdSe-Cysteine-Hg complex through Hg-O and Hg-N bonds hindered the excitation of CdSe resulting in the decrease of the PL intensity (Han et al., 2009; Xia et al., 2008). Meanwhile, the binding between Hg and the capping ligand of CdSe brought Hg close enough to the fluorescent CdSe NPs allowing an effective electron transfer from the excited state of CdSe to Hg ion, which was also responsible for the PL quenching, especially at the higher Hg concentrations (Jin et al., 2004; Chen et al., 2006; Zhu et al., 2017).

4. Conclusions and Environmental Implications

The results of this study provide insight into the behavior of Hg in the environment in the presence of natural or manufactured coated NPs. This is important as the attachment of Hg to particles directly affects its fate and transport in the environment. If Hg and CH_3Hg can be associated with environmental and manufactured NPs that do not have a Hg core, then there is the likelihood that the transport of Hg will be enhanced. As Hg binds strongly to particulates in the environment, Hg is removed from solution with sinking particulate material, being the dominant sink for Hg in many aquatic systems. Having Hg and CH_3Hg bound to NPs could enhance their ability to interact with organisms and be bioaccumulated, in a similar manner that binding to DOC enhances the water column concentrations of Hg and CH_3Hg (Hsu-Kim et al., 2013; Balcom et al., 2015). This study also suggests that there needs to be further consideration of the fact that interactions between metals in solution with the surface of NPs could change their toxicity, as the CdSe-Hg or CdS-Hg NPs would be much more toxic to organisms than those without the associated Hg. Thus, in a manner similar to microplastics that are now ubiquitous in the aquatic environment, and absorb contaminants from solution (Vedolin et al., 2018; Brennecke et al., 2016), association of heavy metals and other contaminants will alter the toxicity of NPs within the environment. Such possibilities need further study.

In particular, the results presented above suggest Hg associated with coated NPs may be more labile if the association is predominantly with the surface ligands. The association with the NPs does not allow for a potentially thermodynamically favorable metal exchange reaction to occur under environmental conditions, even though the following reaction should be highly favorable (Stumm and Morgan, 1996; Mason, 2013):

$$CdS\ (s) + Hg^{2+} = HgS\ (s) + Cd^{2+} \qquad \log K = 25.2 \qquad (5)$$

The reaction would be similarly highly favorable for the Se analog reaction (log K ~ 25). These reactions did not occur in our experiments suggesting that the metal inside the NP core is not readily available for release. As noted above, however, recent studies examining the methylation of Hg in the presence of HgS NPs suggests that the factors controlling methylation in the presence of solids cannot be easily predicted based on solubilization and similar experimental approaches (Zhang et al., 2019; Rivera et al., 2019).

Our results show however that while Hg associated with HgS NPs is within the core of the NP, it is also possible that it is bound to the surface ligands. This is clearly shown by the XPS data. Previous studies have mostly characterized the HgS NPs using XAFS and similar approaches (e.g., Poulin et al., 2017; Rivera et al., 2019; Pham et al., 2014) and these methods determine the overall average association of the Hg in the NP. As noted above, the Hg:Cd ratio in our experiments was always <0.05, and so if the metal of the core of our NPs had been Hg instead of Cd, X-ray-based approaches would likely not have identified correctly that the surface Hg was bound differently than the Hg in the core as the surface Hg would have been a few % at most of the total Hg. We suggest that this surface Hg is likely to be less strongly bound than the Hg within the HgS NP core (bound to inorganic sulfide), or Hg associated with DOC in solution or with natural POC (Hg likely bound to thiols in both situations). In our experiments with the Cd-core NPs, the Hg was found to be associated with the carboxylic and amine groups of the cysteine, and therefore less strongly bound. Clearly, the strength of the association of Hg with the capping agent would be dependent on the capping ligand as there could be thiol sites available if the ligands used had multiple reduced sulfur sites, such as found with natural DOC.

For example, in the experiments of Mazrui et al. (2016), comparing the methylation rate of sediments spiked with inorganic Hg ($HgCl_2$), HgS NPs prepared in a similar manner to those

discussed here, and Hg bound to DOC and POC, the HgS NPs resulted in methylation at a similar rate to the inorganic spike in most of the natural sediments used. Overall, only a few % of the added Hg was methylated during the incubations period and we suggest that the differences in methylation are explained by the likely readily available Hg present on the NP surface, and the small size of the NPs means that there is substantially more surface area available for Hg binding than would be found with a typical micro particle or POC. Most humic material also likely has a higher surface area than typical metal sulfide/selenide NPs. Other studies could be interpreted in a similar manner. Results from experiments with natural sediments are likely different from those obtained with pure cultures and simpler matrices where the association of the methylating organisms and the NPs are much stronger, and much more of the inorganic Hg is methylated during the experiment (Zhang et al., 2019; Pham et al., 2014; Graham et al., 2012).

One further implication of our study is suggested by the fact that exchange did not occur in our experiments until a very high concentration of Hg had been added to the solution with CdSe NPs. This suggests that the mobility of the Cd and the exchange reaction is hindered by the stability of the NP, and that this would also likely be the case for HgS NPs as well. Indeed, Mazrui et al. (2018) found that while HgS NPs capped with cysteine or natural DOC were stable for months in the dark under anoxic conditions, they coagulated more readily under oxic conditions and light. The changes were mostly a result of coagulation that impacted the apparent size of HgS NPs within days, depending on the exact nature of the experiment. But the overall specific UV absorbance (SUVA) of the DOC did not change suggesting the changes were not due to degradation of the NPs but mostly due to coagulation. This effect may account for the impact of "ageing" of HgS NPs (Zhang et al., 2012), which decreased the methylation rate in laboratory studies as coagulation increases the aggregate size. There may also be changes in the speciation of the Hg associated with the capping agent over time as well (Poulin et al., 2017) although this was not examined in this study.

Another aspect of the environmental fate of NPs is related to their reactivity. While many NPs are much more reactive than their micro counterparts it is likely that the HgS NPs are not as reactive in terms of CH_3Hg transformations as uncoated micro HgS. Jonsson et al. (2016) found that it was possible for a reaction to occur on the surface of HgS, as well as FeS and CdS micro particles, that lead to the conversion of CH_3Hg into $(CH_3)_2Hg$ with the precipitation of HgS. Two

514 CH_3Hg molecules on the solid surface, bound to surface S atoms, were involved in a methyl
515 exchange reaction, with the driving force being the precipitation of HgS. This reaction can be
516 formulated as:

517 $$CH_3Hg\text{-}S\text{-}R\text{-}S\text{-}HgCH_3 = (CH_3)_2Hg + HgS_2\text{-}R\ (s)$$

518 and the precipitation of the HgS would make the reaction highly favorable. Given the results
519 discussed above, this reaction is unlikely to occur in the presence of HgS NPs, or any other
520 sulfide NPs, prepared in the manner they generally are with a thiol-containing capping agent, and
521 as used in our experiments. The micro particles used by Jonsson et al. (2016) were not "capped"
522 with an organic ligand, so the CH_3Hg could bind directly with a sulfide ion on the surface of the
523 particle. Only at high concentrations of Hg or CH_3Hg in solution would the ions penetrate the
524 outer surface and interact with the core of the NP. In our experiments, this led to precipitation of
525 HgS or HgSe. Such a result is consistent with other findings that it is possible to form NPs with
526 two metal ions (e.g. Cd and Hg) through a cation exchange reaction when the ratio of Hg in
527 solution is high relative to the amount of Cd in the NP – above 0.1 Hg:Cd, or if the reactions are
528 completed in non-aqueous media (Gupta et al., 2013; Choi et al., 2017). Furthermore, in the
529 experiments of Skyllberg and Drott (2010), at lower ratios (0.002-0.012 Hg:Fe), Hg precipitated
530 on the surface of FeS micro particles rather than exchanging with the Fe or being complexed to
531 the surface sulfides. Such precipitation of HgS likely occurred during the conversion of CH_3Hg
532 to $(CH_3)_2Hg$ in the experiments of Jonsson et al. (2016). Similar reactions would occur on the
533 surface of uncoated metal-sulfide/selenide NPs, which could form at higher temperature and Hg
534 concentrations, perhaps in hydrothermal vents. These summations need to be examined further.
535 Additionally, the presence of uncoated NPs in aquatic environments may be limited given the
536 likelihood that they would readily become coated with natural organic matter.

537 Overall, our study provides a detailed explanation for the interaction of metal ions with the
538 surface of natural or manufactured NPs that contain a metal-sulfide/selenide core, and how this
539 affects their reactivity and fate and transport in the environment. The Hg and CH_3Hg adsorbed to
540 such NPs is not bound in a similar manner to the core metal ions and we suggest these would be
541 readily bioavailable to (de)methylating organisms or for bioaccumulation into the food chain.

542

Acknowledgements

The help of undergraduate students in the studies detailed in this paper is acknowledged, especially the work of Steve Kolakowski, a Chemistry undergraduate student at Storrs. The authors all contributed substantially to the research and the data interpretation and paper writing. Results from these studies formed part of the PhD thesis research of Nashaat Mazrui and Xudong Wang. The project was funded by the National Science Foundation Environmental Chemical Science program through award # 1607913 to Mason and Zhao.

References

Asaduzzaman, A.M., Khan, M.A.K., Schreckenbach, G. and Wang, F., 2010. *Computational studies of structural, electronic, spectroscopic and thermodynamic properties of methylmercury-amino acid complexes and their Se analogues*. Inorganic Chemistry, 49(3): 870-878.

Balcom, P.H., et al., *Sources of water column methylmercury across multiple estuaries in the Northeast U.S.* Marine Chemistry, 2015. **177**: p. 721-730.

Benoit, J.M., et al., *Geochemical and biological controls over methylmercury production and degradation in aquatic ecosystems*, in *Biogeochemistry of Environmentally Important Trace Elements*. 2003. p. 262-297.

Brennecke, D., et al., *Microplastics as vector for heavy metal contamination from the marine environment.* Estuarine, Coastal and Shelf Science, 2016. **178**: p. 189-195.

Chen, J., et al., *A novel fluorescent array for mercury (II) ion in aqueous solution with functionalized cadmium selenide nanoclusters.* Analytica Chimica Acta, 2006. **577**(1): p. 77-84.

Choi, D., et al., *Major electronic transition shift from bandgap to localized surface plasmon resonance in Cd x Hg 1-x Se Alloy Nanocrystals.* Chemistry of Materials, 2017. **29**(19): p. 8548-8554.

Craig, P. and Bartlett, P., 1978. *The role of hydrogen sulfide in environmental transport of mercury*. Nature, 275: 635-638.

571 Ding, X., et al., *A highly selective and simple fluorescent sensor for mercury (II) ion detection*
572 *based on cysteamine-capped CdTe quantum dots synthesized by the reflux method.*
573 Luminescence, 2015. **30**(4): p. 465-471.
574 Driscoll, C.T., et al., *Mercury as a Global Pollutant: Sources, Pathways, and Effects.*
575 Environmental Science & Technology, 2013. **47**(10): p. 4967-4983.
576 Duan, J., L. Song, and J. Zhan, *One-pot synthesis of highly luminescent CdTe quantum dots by*
577 *microwave irradiation reduction and their Hg 2+ -sensitive properties.* Nano Research,
578 2009. **2**(1): p. 61-68.
579 Fraiji, L.K., D.M. Hayes, and T.C. Werner, *Static and dynamic fluorescence quenching*
580 *experiments for the physical chemistry laboratory.* Journal of Chemical Education, 1992.
581 **69**(5): p. 424-428.
582 Gilmour, C.C., et al., *Mercury Methylation by Novel Microorganisms from New Environments.*
583 Environmental Science & Technology, 2013. **47**(20): p. 11810-11820.
584 Graham, A.M., G.R. Aiken, and C.C. Gilmour, *Effect of dissolved organic matter source and*
585 *character on microbial Hg methylation in Hg-S-DOM solutions.* Environmental Science and
586 Technology, 2013. **47**(11): p. 5746-5754.
587 Gupta, S., et al., *Cd x Hg (1-x) Te alloy colloidal quantum dots: Tuning optical properties from*
588 *the visible to near-infrared by ion exchange.* Particle and Particle Systems Characterization,
589 2013. **30**(4): p. 346-354.
590 Han, B., J. Yuan, and E. Wang, *Sensitive and selective sensor for biothiols in the cell based on*
591 *the recovered fluorescence of the CdTe quantum dots-Hg(II) system.* Analytical Chemistry,
592 2009. **81**(13): p. 5569-5573.
593 Hofacker, A.F., et al., *Mercury mobilization in a flooded soil by incorporation into metallic*
594 *copper and metal sulfide nanoparticles.* Environmental Science and Technology, 2013.
595 **47**(14): p. 7739-7746.
596 Hsu-Kim, H., et al., *Mechanisms regulating mercury bioavailability for methylating*
597 *microorganisms in the aquatic environment: A critical review.* Environmental Science and
598 Technology, 2013. **47**(6): p. 2441-2456.
599 Jeong, H.Y., Klaue, B., Blum, J.D. and Hayes, K.F., 2007. *Sorption of mercuric ion by synthetic*
600 *nanocrystalline mackinawite (FeS)*. Environmental Science and Technology, 41(22):
601 7699-7705.

Jeong, H.Y., Sun, K. and Hayes, K.F., 2010. *Microscopic and spectroscopic characterization of Hg(II) immobilization by mackinawite (FeS)*. Environmental Science and Technology, 44(19): 7476-7483.

Khan, M.A.K. and Wang, F.Y., 2010. *Chemical demethylation of methylmercury by selenoamino acids*. Chemical Research in Toxicology, 23(7): 1202-1206.

Jin, W.J., et al., *Surface-modified CdSe quantum dots as luminescent probes for cyanide determination.* Analytica Chimica Acta, 2004. **522**(1): p. 1-8.

Jing, L., et al., *Aqueous Based Semiconductor Nanocrystals.* Chemical Reviews, 2016. **116**(18): p. 10623-10730.

Jonsson, S., et al., *Mercury Methylation Rates for Geochemically Relevant Hg-II Species in Sediments.* Environmental Science & Technology, 2012. **46**(21): p. 11653-11659.

Jonsson, S., N.M. Mazrui, and R.P. Mason, *Dimethylmercury Formation Mediated by Inorganic and Organic Reduced Sulfur Surfaces.* Scientific Reports, 2016. **6**.

Mahaffey, K.R., et al., *Balancing the benefits of n-3 polyunsaturated fatty acids and the risks of methylmercury exposure from fish consumption.* Nutrition Reviews, 2011. **69**(9): p. 493-508.

Manceau, A., et al., *Formation of Mercury Sulfide from Hg(II)-Thiolate Complexes in Natural Organic Matter.* Environmental Science and Technology, 2015. **49**(16): p. 9787-9796.

Mason, R.P., *Trace Metals in Aquatic Systems*. 2013, Chichester: John Wiley-Blackwell. 431.

Mazrui, N.M., et al., *Enhanced availability of mercury bound to dissolved organic matter for methylation in marine sediments.* Geochimica et Cosmochimica Acta, 2016. **194**: p. 153-162.

Mazrui, N.M., et al., *The precipitation, growth and stability of mercury sulfide nanoparticles formed in the presence of marine dissolved organic matter.* Environmental Science: Processes and Impacts, 2018. **20**(4): p. 642-656.

Mazrui, N.M., *The Interaction of Mercury and Methylmercury with Reduced Sulfur in the Environment: Implications for Mercury and Methylmercury Transformations* in *Chemistry*. 2016, University of Connecticut. p. 176.

Ndu, U., et al., *Quantification of Mercury Bioavailability for Methylation Using Diffusive Gradient in Thin-Film Samplers.* Environmental Science and Technology, 2018. **52**(15): p. 8521-8529.

Outridge, P.M., et al., *Updated Global and Oceanic Mercury Budgets for the United Nations Global Mercury Assessment 2018.* Environmental Science and Technology, 2018. **52**(20): p. 11466-11477.

Paim, A.P.S., et al., *Fluorescence probe for mercury(II) based on the aqueous synthesis of CdTe quantum dots stabilized with 2-mercaptoethanesulfonate.* New Journal of Chemistry, 2017. **41**(9): p. 3265-3272.

Park, Y.S., et al., *Aqueous phase synthesized CdSe nanoparticles with well-defined numbers of constituent atoms.* Journal of Physical Chemistry C, 2010. **114**(44): p. 18834-18840.

Pham, A.L.T., et al., *Precipitation of nanoscale mercuric sulfides in the presence of natural organic matter: Structural properties, aggregation, and biotransformation.* Geochimica et Cosmochimica Acta, 2014. **133**: p. 204-215.

Podar, M., et al., *Global prevalence and distribution of genes and microorganisms involved in mercury methylation.* Science Advances, 2015. **1**.

Poulin, B.A., et al., *Effects of Sulfide Concentration and Dissolved Organic Matter Characteristics on the Structure of Nanocolloidal Metacinnabar.* Environmental Science and Technology, 2017. **51**(22): p. 13133-13142.

Regnell, O. and C.J. Watras, *Microbial Mercury Methylation in Aquatic Environments: A Critical Review of Published Field and Laboratory Studies.* Environmental Science and Technology, 2019. **53**(1): p. 4-19.

Rivera, N.A., Jr., P.M. Bippus, P.M. and H. Hsu-Kim, *Relative reactivity and bioavailability of mercury sorbed to or coprecipitated with aged iron sulfides*. Environ. Sci. Technol., 2019, **53:** 7391-7399.

Schartup, A.T., et al., *Methylmercury Production in Estuarine Sediments: Role of Organic Matter.* Environmental Science & Technology, 2013. **47**(2): p. 695-700.

Schartup, A.T., P.H. Balcom, and R.P. Mason, *Sediment-Porewater Partitioning, Total Sulfur, and Methylmercury Production in Estuaries.* Environmental Science & Technology, 2014. **48**(2): p. 954-960.

Skyllberg, U. and A. Drott, *Competition between disordered iron sulfide and natural organic matter associated thiols for mercury(II) - An EXAFS study.* Environmental Science and Technology, 2010. **44**(4): p. 1254-1259.

Slowey, A.J. and Brown, G.E., 2007. *Transformations of mercury, iron, and sulfur during the reductive dissolution of iron oxyhydroxide by sulfide*. Geochimica Et Cosmochimica Acta, 71(4): 877-894.

Stumm, W. and J.J. Morgan, *Aquatic Chemistry*. 1996, New York: John Wiley and Sons.

Sunderland, E.M., M. Li, and K. Bullard, *Decadal changes in the edible supply of seafood and methylmercury exposure in the United States.* Environmental Health Perspectives, 2018. **126**(1).

Van Leeuwen, H.P., et al., *Chemodynamics and bioavailability of metal ion complexes with nanoparticles in aqueous media.* Environmental Science: Nano, 2017. **4**(11): p. 2108-2133.

Vedolin, M.C., et al., *Spatial variability in the concentrations of metals in beached microplastics.* Marine Pollution Bulletin, 2018. **129**(2): p. 487-493.

Wu, N., et al., *Interaction of Fatty Acid Monolayers with Cobalt Nanoparticles.* Nano Letters, 2004. **4**(2): p. 383-386.

Xia, Y.S. and C.Q. Zhu, *Use of surface-modified CdTe quantum dots as fluorescent probes in sensing mercury (II).* Talanta, 2008. **75**(1): p. 215-221.

Yu, K., *CdSe Magic-Sized Nuclei, Magic-Sized Nanoclusters and Regular Nanocrystals: Monomer Effects on Nucleation and Growth.* Adv. Mat., 2012. **24**: p. 1123-1132.

Yu, W.W., et al., *Experimental determination of the extinction coefficient of CdTe, CdSe, and CdS nanocrystals.* Chemistry of Materials, 2003. **15**(14): p. 2854-2860.

Zahir, F., et al., *Low dose mercury toxicity and human health.* Environmental Toxicology and Pharmacology, 2005. **20**(2): p. 351-360.

Zhang, S., et al., *Aggregation, dissolution, and stability of quantum dots in marine environments: Importance of extracellular polymeric substances.* Environmental Science and Technology, 2012. **46**(16): p. 8764-8772.

Zhang, T., et al., *Net methylation of mercury in estuarine sediment microcosms amended with dissolved, nanoparticulate, and microparticulate mercuric sulfides.* Environmental Science and Technology, 2014. 4**8**(16): p. 9133-9141.

Zhang, L., S. Wu, L. Zhao, X. Lu, E.M. Pierce and B. Gu, *Mercury sorption and desorption on organo-mineral particulates as a source of microbial methylation*. Environ. Sci. Technol, 2019, **53**: 2426-2433.

Zhu, J., et al., *CdTe quantum dot-based fluorescent probes for selective detection of Hg (II): The effect of particle size.* Spectrochimica Acta - Part A: Molecular and Biomolecular Spectroscopy, 2017. **177**: p. 140-146.

Figures and Tables

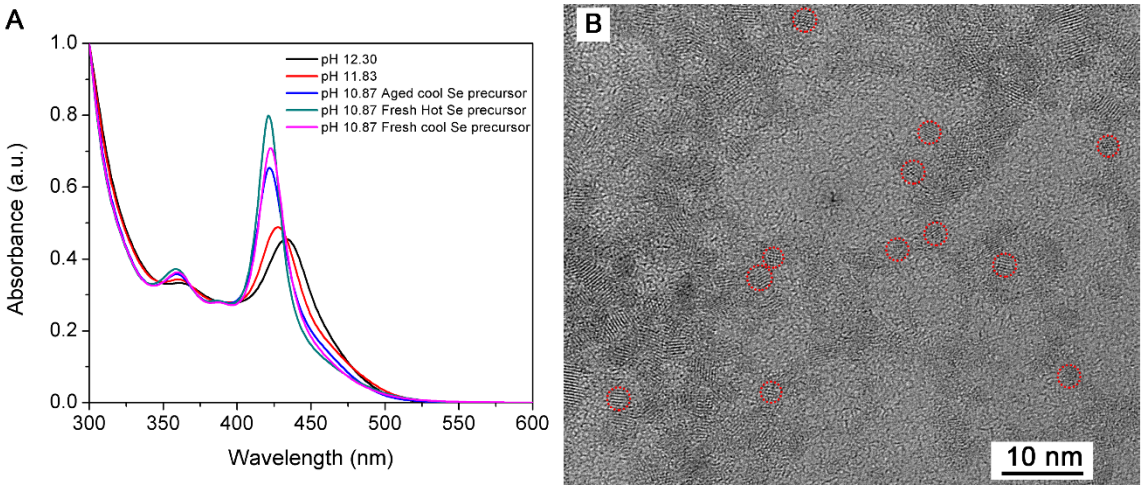

Figure 1. (A)UV-Vis spectra of CdSe nanoparticles prepared with different pH and aging of the Se precursor; (B) the TEM image of CdSe nanoparticles.

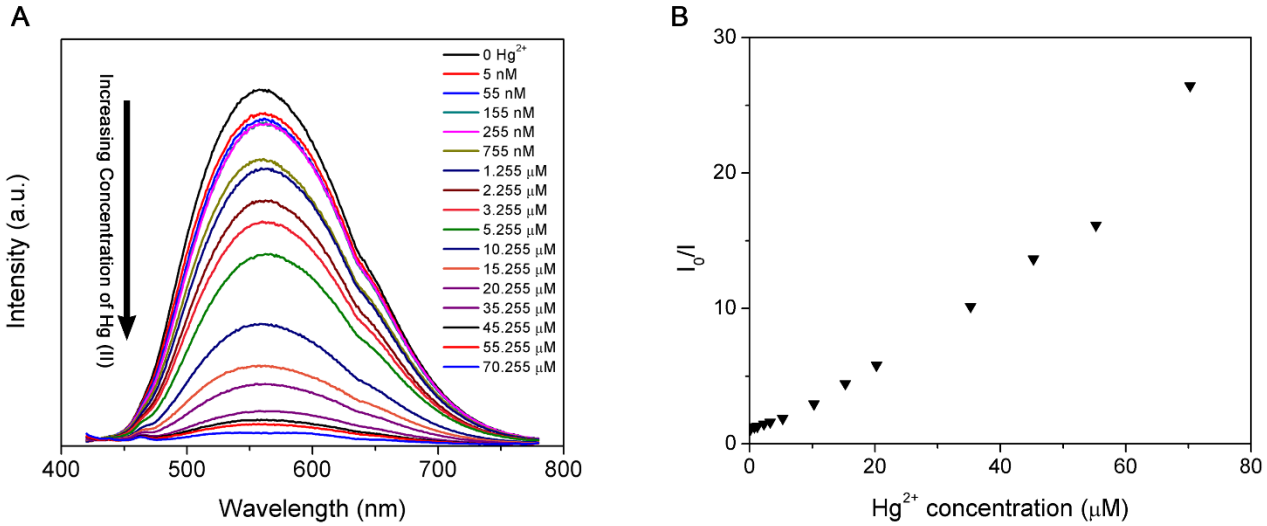

Figure 2. (A) PL spectra of CdSe nanoparticle solution with different concentration of $HgCl_2$; (B) the Stern-Volmer fitting of the data in the spectra. The concentrations of Hg added ranged from 5 nM to 70 µM and were added to separate CdSe solutions prior to their analysis by fluorescence.

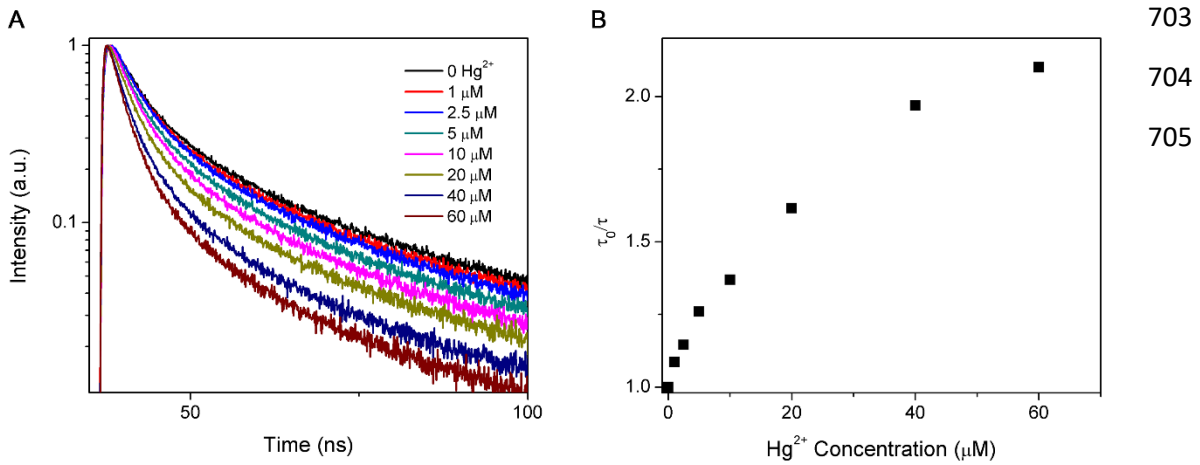

Figure 3. (A) PL decay of CdSe nanoparticle solution with different concentrations of $HgCl_2$; (B) the Stern-Volmer fitting of the data in the PL decay for the CdSe nanoparticles. The samples run were a subset of those analyzed by fluorescence and at the higher concentration range.

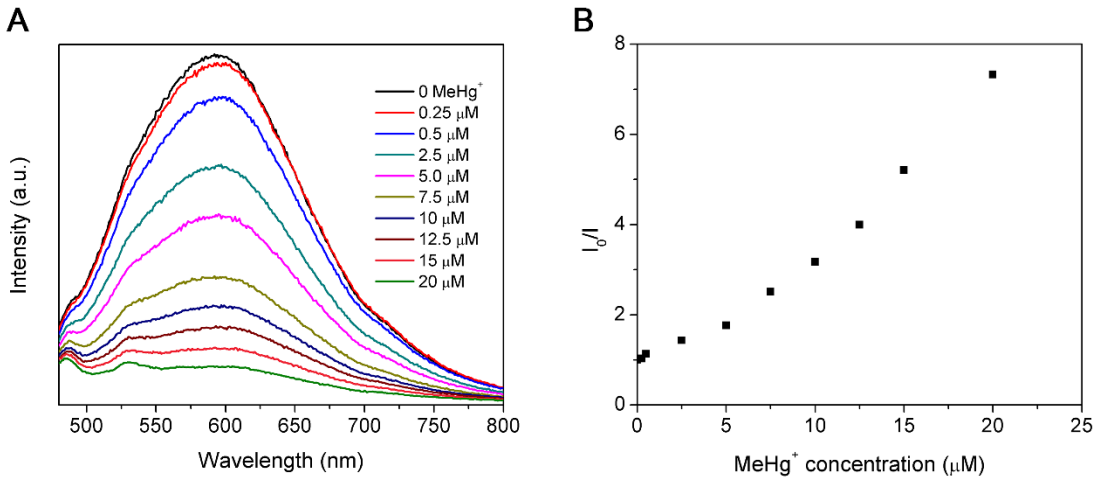

Figure 4. (A) PL spectra of CdSe nanoparticle solution with different concentration of CH_3HgCl; (B) the Stern-Volmer fitting of the data in the spectra. The concentrations of CH_3Hg added ranged from 250 nM to 20 μM and were added to separate CdSe solutions prior to their analysis by fluorescence.

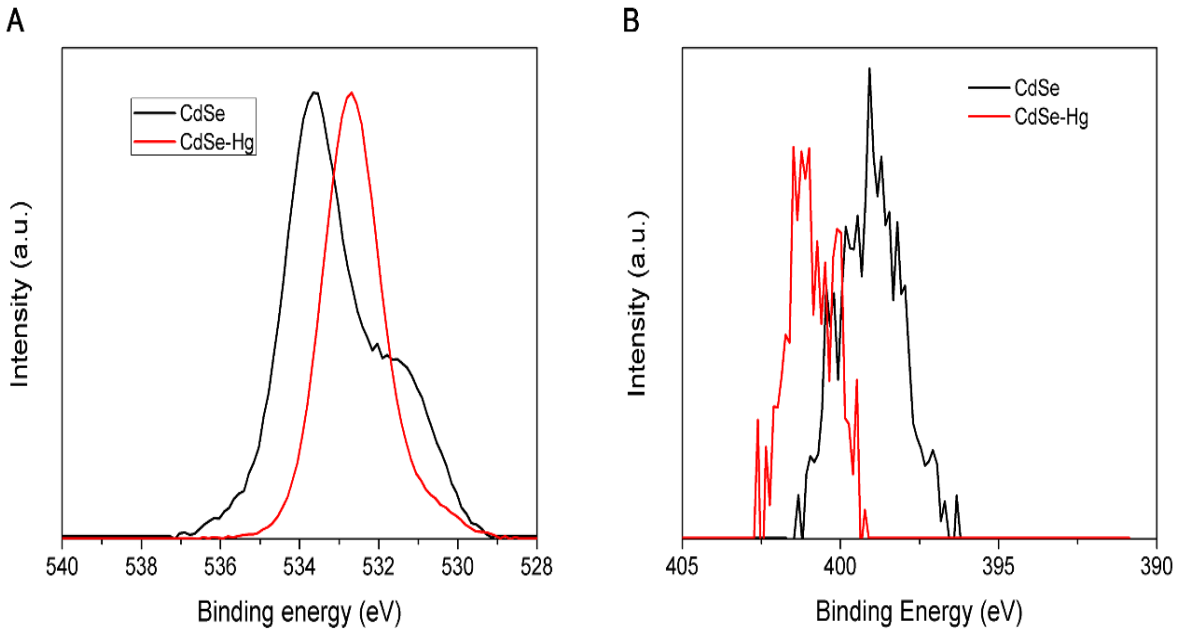

Figure 5. XPS spectra of O 1s (A) and N 1s (B) of CdSe nanoparticles with (red) and without (black) the addition of $HgCl_2$.

706

707

708 *Table 1. Relative amounts of cadmium and mercury in the supernatant solution and in the*
709 *"pellet" after centrifugation of the CdSe plus mercury nanoparticulate solutions. Calcium*
710 *chloride was added to enhance precipitation of the nanoparticles during centrifugation. See*
711 *Methods for details of the experiment.*

Sample	**Hg in Particles (µM)**	**Hg in Solution (µM)**	**% Hg in Particles.**	**Cd in Particles (µM)**	**Cd in Solution (µM)**	**% Cd in Particles**
no added Hg	DL	1.7×10^{-4}	-	2019	21	99.4
Spike #1	DL	4.8×10^{-4}	-	806	14	98.3
Spike #2	0.019	9.3×10^{-4}	95.3	868	9	99.0
Spike #3	0.11	1.5×10^{-3}	98.6	1003	11	98.9
Spike #4	0.20	3.7×10^{-4}	99.8	923	11	98.9
Spike #5	35.1	0.24	99.3	590	*	-
10 µM Hg stock	0.21	9.21	2.3	DL	*	-

712 *Notes: DL = detection limit; * = supernatant or precipitation samples were not run*

713

714

Supporting Information

The Synthesis of Aqueous CdS Nanoparticles

Cysteine capped CdS NPs were synthesized with the addition of L-cysteine, Cd^{2+} and sulfide to N_2 degassed 2.2 mM $NaHCO_3$ buffer (pH 7.8) in the order mentioned. The cysteine solution was prepared and stored in a glove box prior to use, and was added to the buffer to obtain a final concentration of 600 µM. Cd^{2+} was added to obtain a concentration of 150 µM. A sulfide stock solution was prepared by dissolving 10 g of sodium sulfide nanohydrate in 5 mL of degassed water and its concentration was determined by titration with $Pb(NO_3)_2$ using an Orion ion selective electrode. It was added to the solution to obtain a final concentration of 75 µM as described in our previous studies (Mazrui et al., 2018). The solution was aged for three days and purified using centrifugation before use in the titration experiments.

Instrumentation

The transmission electron microscopy (TEM) images were taken with a Thermo Fisher-Talos electron microscope at an accelerating voltage of 200 kV.

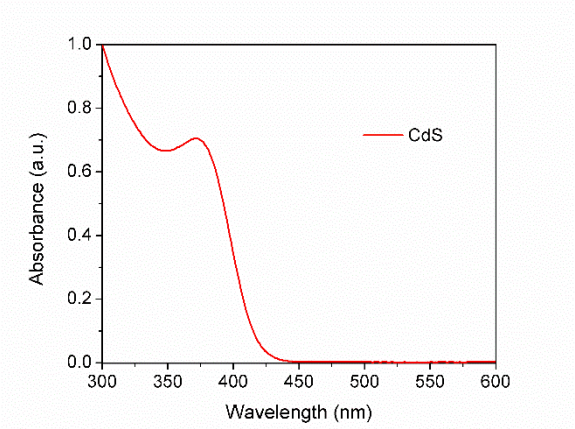

Figure S1. *The UV-Vis spectrum of the CdS nanoparticles.*

732

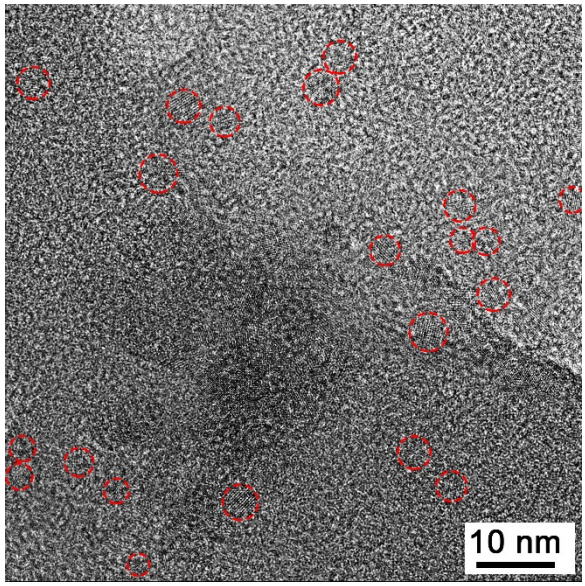

Figure S2. *The TEM image of the CdS nanoparticles.*

733

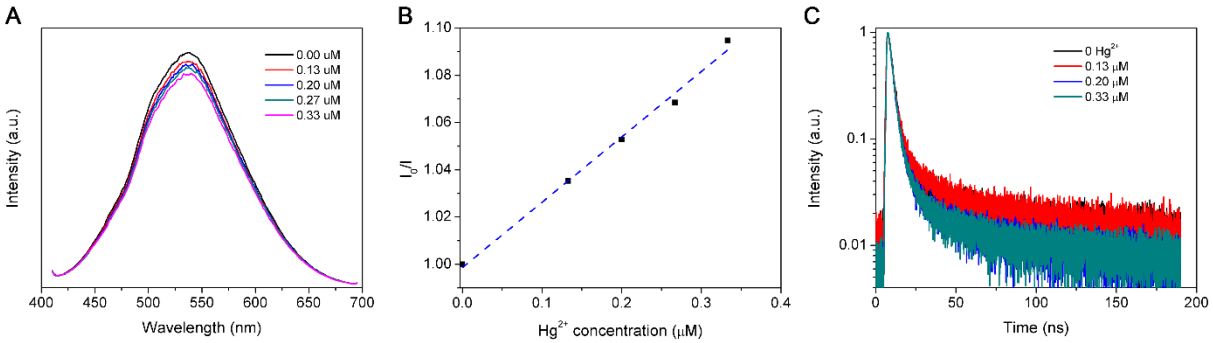

Figure S3. *(A) The PL spectra of the CdS nanoparticle solution with different concentrations of* $HgCl_2$ *added; (B) the Stern-Volmer fitting of the data in the spectra; and (C) the decay plots for the Hg-CdS nanoparticles studies.*

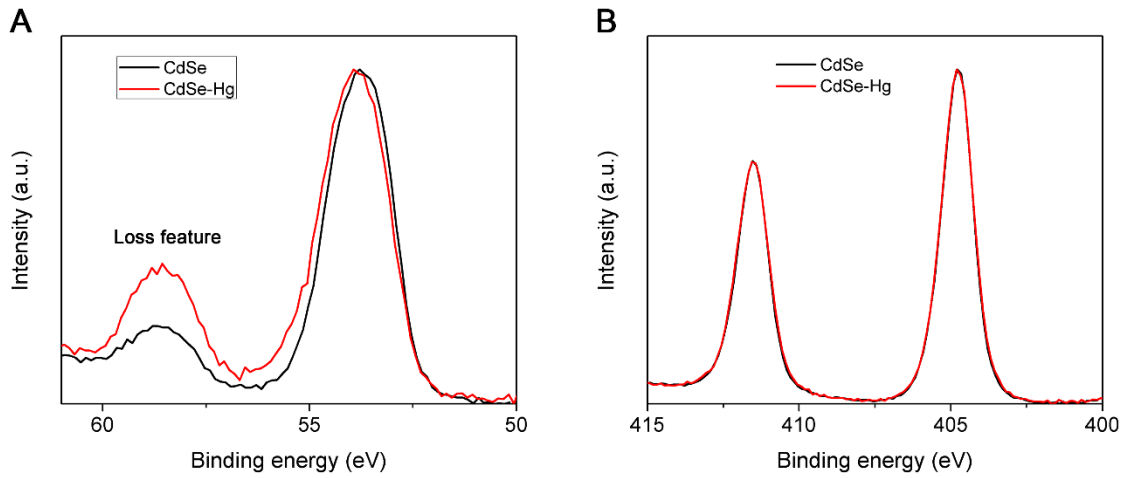

Figure S4. *XPS spectra of Se 3d (A) and Cd 3d (B) of CdSe nanoparticles with (red) and without (black) the addition of Hg (II).*

Table S1. *Formation constants for inorganic mercury and methylmercury for inorganic and organic ligands for the following reaction:* $M^{n+} + L^{m-} = LM^{n-m}$. *Taken from the literature (Stumm and Morgan, 1996; Foti et al., 2009; Cataldo et al., 2012; Hojo et al., 1977; Libich and Rabenstein, 1973; Reid and Rabenstein, 1982).*

Ligand (L)	Logβ Hg^{2+}	Logβ CH_3Hg^+	Ligand (L)	Logβ Hg^{2+}	Logβ CH_3Hg^+
OH^-	10.6	9.37	Cysteine	15.3	11.6
Cl^-	7.2	5.3	Mercaptoethylene	11.1	16.1
Acetic	3.7	3.2	Mercaptoacetic acid	11.5	16.9
Glycine	10.9	7.9	Thioglycolate		16.7
EDTA	23.5	10.0	Dimethylamine		7.8
NTA	15.9	9.0	Ethylenediamine	14.3	
			Dimethylenediamine		5.5

References

1. Cataldo, S., et al., *Sequestration of (CH 3)Hg + by amino-polycarboxylic chelating agents.* Journal of Molecular Liquids, 2012. **172**: p. 46-52.

2. Foti, C., et al., *Interaction of inorganic mercury(II) with polyamines, polycarboxylates, and amino acids.* Journal of Chemical and Engineering Data, 2009. **54**(3): p. 893-903.

3. Hojo, Y., Y. Sugiura, and H. Tanaka, *Chelate and non-chelate complexes of organomercury with polymethylenediamines.* Journal of Inorganic and Nuclear Chemistry, 1977. **39**(4): p. 715-720.

4. Libich, S. and D.L. Rabenstein, *Nuclear Magnetic Resonance Studies of the Solution Chemistry of Metal Complexes Determination of Formation Constants of Methylmercury Complexes of Selected Carboxylic Acids.* Analytical Chemistry, 1973. **45**(1): p. 118-124.

5. Reid, R.S. and D.L. Rabenstein, *Nuclear Magnetic Resonance Studies of the Solution Chemistry of Metal Complexes. 19. Formation Constants for the Complexation of Methylmercury by Glutathione, Ergothioneine, and Hemoglobin.* Journal of the American Chemical Society, 1982. **104**(24): p. 6733-6737.

6. Stumm, W. and J.J. Morgan, *Aquatic Chemistry*. 1996, New York: John Wiley and Sons.

758

759